

Research paper

The study of a novel magnetic crankshaft

Junnan Wang^{a,*}, Yaodong Wang^b^a Nanjing Vocational University of Industry Technology, Nanjing 210023, China^b Department of Engineering, Durham University, Durham DH1 3LE, UK

ARTICLE INFO

Keywords:

Energy storage
Magnetic crankshaft
Magnetic lead screw
3D finite element analysis

ABSTRACT

This paper introduces a revolutionary mechanism, the Four-Translator Magnetic Crankshaft (FTMC), designed to address inherent limitations of the Magnetic Lead Screw (MLS) in energy storage and driving efficiency. The FTMC combines features of the MLS and a traditional cross crankshaft, enabling efficient energy conversion between continuous rotatory motions and reciprocating linear motions. The study presents the FTMC's working principle, theoretical calculations, 3D finite element analysis (FEA) validation, and comprehensive performance analyses. The FTMC's rotor, featuring a unique magnet array, allows for continuous rotation while the four translators reciprocate with a 90-degree phase difference. This breakthrough resolves the energy storage challenge faced by MLS, leading to enhanced efficiency and frequency. The paper explores the FTMC's static and dynamic performance, demonstrating its superiority in achieving 4.6 times higher reciprocating speeds or 93.3 % lower driving torque compared to the same-sized MLS in the limiting case. Furthermore, the study proposes an innovative assembly design with a 2-air gap topology, addressing potential radial attraction issues and reducing translator mass. The anticipated performance under ideal conditions, based on 3D FEA results, showcases the FTMC's ability to transmit about 1.4 kW power with efficiencies exceeding 75 % at rated load angles and 30 Hz driving frequencies. Theoretical insights into the FTMC's capabilities open promising avenues for future research and prototyping. Experimental validation is recommended to confirm the mechanism's maximum driving ability, offering significant advancements in Magnetic Lead Screw and high-speed magnetic drive systems. Future studies should focus on prototype manufacturing and controllable load test bench design to validate the presented theoretical analysis.

1. Introduction

The Magnetic Lead Screw (MLS) (Mustafa et al., 2023,) is a branch of the magnetic gear (Lorimer and Hartman, 1997), facilitating energy conversion between low-speed, high-thrust linear motion and high-speed, low-torque rotational motion (and vice versa).

The working principle of the MLS is similar to that of a mechanical lead screw. As shown in Fig. 1, the rotor can be seen as a stud, the translator as a nut, and the helically distributed magnet can be seen as a lead screw tooth. A lot of studies about the MLS are being carried out due to the contactless feature of its magnetic coupling structure, which contributes to less mechanical loss and higher driving speed compared to the traditional ball screw structure. The current research hotspot about the MLS mainly focuses on the magnetic field design and size optimisation which aims to increase the driving ability, namely the higher MLS static maximum thrust with lighter moving component mass. Literature (Wang et al., 2011) provided a mathematical solution to

estimate the MLS flux density distribution and uses the equivalent current density to calculate the thrust at different positions of the translator. A more detailed comparative analysis of MLS with different magnet topologies and sizes was carried out in (Holm et al., 2013). The concept of segmented magnets was introduced in (Jenney and Pakdelian, 2020) to counter the unbalanced forces caused by manufacturing deviations of helical structure magnets. In (Safarpour and Pakdelian, 2022), a reluctance MLS was studied and different slot structures coupled with Quasi-Halbach magnet arrays were discussed. Most of the above typical studies are about improving the static maximum thrust of the MLS, namely the thrust acting on the translator with a 90-degree load angle. Although increasing the static thrust can indirectly improve the driving capacity of the MLS, it essentially fails to change the status quo that the mechanism does not have beneficial energy storage characteristics. Specifically, when the MLS translator carries out reciprocating motion, its rotor will also carry out clockwise and anticlockwise rotary motion simultaneously, namely the rotor inertia not only cannot store energy

* Corresponding author.

E-mail address: b2024383@gmail.com (J. Wang).<https://doi.org/10.1016/j.egy.2024.06.032>

Received 5 February 2024; Received in revised form 29 April 2024; Accepted 14 June 2024

Available online 27 June 2024

2352-4847/© 2024 The Authors. Published by Elsevier Ltd. This is an open access article under the CC BY license (<http://creativecommons.org/licenses/by/4.0/>).

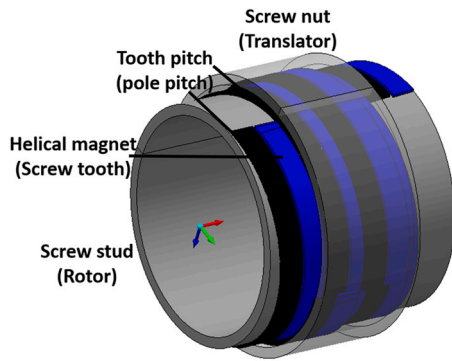


Fig. 1. Magnetic lead screw (MLS).

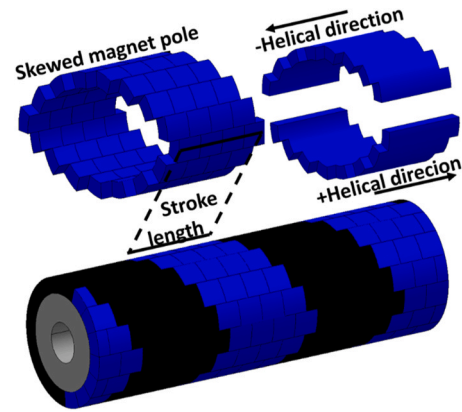


Fig. 3. Rotor magnet array detailed view.

but also needs to consume other forms of energy to offset its kinetic energy.

In this study, the author developed a Four-Translator Magnetic Crankshaft (FTMC) mechanism, which can be applied to high-speed linear driving platforms (Guo et al., 2018) and driving devices for free piston engines (Wang and Baker, 2018). The key novelty of the FTMC is that the FTMC fundamentally solves the problem of rotor energy storage, realizing that the rotor can maintain unidirectional rotation while the translator is moving in reciprocation, thus achieving better efficiency and frequency than the MLS. The basic structure of the FTMC is shown in Fig. 2, when the rotor rotates in a single direction, the four translators will reciprocate with a phase difference of 90 degrees to each other, and the stator is mainly responsible for providing the field flux loop and the translator guide rail. The driving of the FTMC has a bidirectional characteristic, taking the working process of a two-stroke free piston power generation system (Thi et al., 2020) as an example: assuming that the left side of the rotor is connected to the electric machine and the right side of the translator is connected to the free piston, there are two working states. State 1: the torque flows into the FTMC rotor, and translators export reciprocating linear motion to the engine piston, the electric machine is now working as a motor (starting process). State 2: the engine piston thrust flows into FTMC translators in turns to accelerate the rotor in one direction (air intake work process), meanwhile, the rebounding of each translator is completed by the energy stored in the rotor (exhaust compression process), and the electric machine is working as a generator.

2. Material and methods

2.1. Working principle

The rotor magnet array of the FTMC is illustrated in Fig. 3. This array comprises small magnet units with radial magnetization, distinguished by two different colors representing distinct polarities. The arrangement of adjacent magnet units is staggered by half-width, forming an enclosed

skewed magnet pole. This skewed magnet pole structure imitates the “cam-tracks” utilized in the most revolutionary 1-stroke engine from INN Engine Company (Csere, 2023), also similar to the shaped channels on the shifting drum utilized in motorcycles (Maia et al., 2014), with its pole span reflecting the linear stroke length, plays a crucial role when the rotor is in motion. As the rotor undergoes rotation, the skewed magnet pole generates two magnetic field components in the air gap: rotation and oscillation. The rotational component manifests as torque, while the oscillation component manifests as thrust. Notably, the skewed magnet pole is functionally equivalent to that of the MLS, with half of it featuring a positive helical magnet array and the other half a negative helical magnet array, connected end to end. The distinctive rotating and oscillating magnetic field characteristics of the FTMC’s rotor enable continuous rotation while the translator undergoes reciprocating linear motion. This unique feature sets the FTMC apart from conventional MLS systems.

The translator magnet arrangement of the FTMC is depicted in Fig. 4, showcasing four characteristic instants labeled a-d. During instant a, translator 1 aligns axially at position I, while translator 2 is at position II, translator 3 is at position III (equivalent to position I), and translator 4 is at position IV. As the rotor rotates anticlockwise, translator 1 follows a periodic reciprocating motion path of I→II→III→IV→I. Simultaneously, translator 2 follows the path of II→III→IV→I→II, translator 3 follows III→IV→I→II→III, and translator 4 follows IV→I→II→III→IV. Conversely, with clockwise rotor rotation, all four translators reciprocate in the opposite arrow direction pattern. In essence, the four translators reciprocate with a 90-degree phase difference while the rotor continuously rotates 360 degrees.

The operational principle of the FTMC closely resembles that of a piston connecting rod dragging a cross crankshaft. Furthermore, due to the translator moving along the rotor shaft, as opposed to a mechanical crankshaft where the rotor shaft is vertical to the translator, the FTMC eliminates the need for moving joints (piston pins, connecting rod upper and lower bearings, split shaft bushings, fixing bolts, etc.) (Bo et al., 2022), this results in a simpler and more integrated structure.

The driving capability of the FTMC is determined by the relative position between the rotor and the translator, namely, the load angle δ . Fig. 5 shows the magnetic field distribution under different load angles corresponding to the four characteristic instants (a-d). Taking translator 1 for instance, assume the initial position of translator 1 is at position I. When the load angle is set at 0 degrees, the rotor absolute angle is 0 degrees with instant a, 90 degrees with instant b, 180 degrees with instant c and 270 degrees with instant d. The translator thrust and torque are always 0, thus does not have any driving ability. Taking the load angle of 45 degrees as an example, the rotor’s absolute angle is always 45 degrees ahead of the “0-degree” situation which means it can reciprocate drive the translator. The maximum driving ability of the FTMC is attained when the load angle is at 90 degrees. In the actual

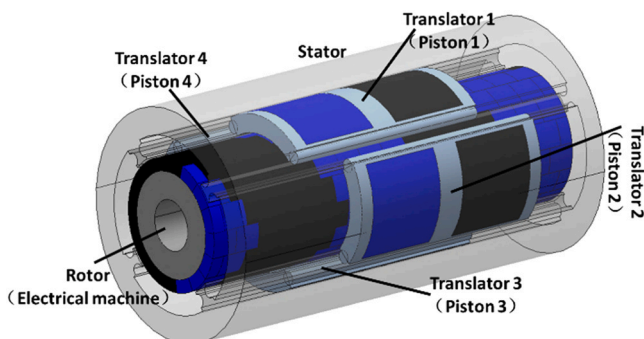


Fig. 2. Four-translator magnetic crankshaft (FTMC).

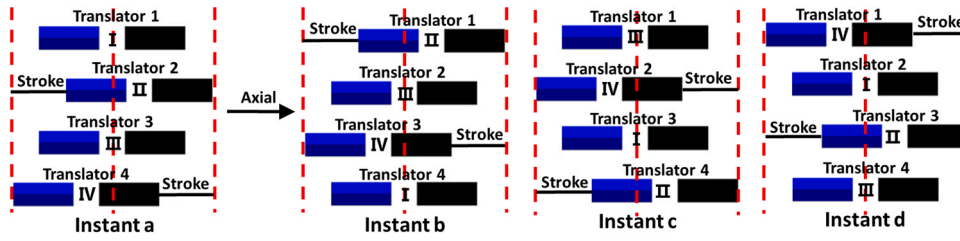


Fig. 4. Translator magnet array at four characteristic instants.

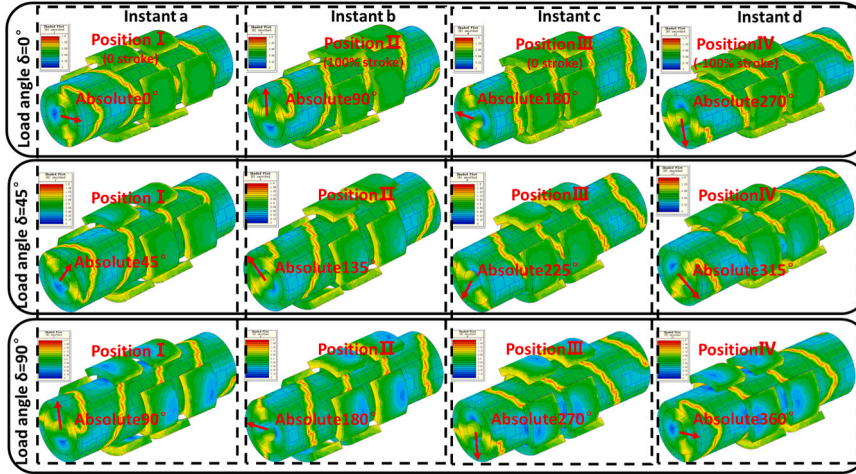


Fig. 5. Load angle and absolute angle.

driving process, the load angle always adjusts itself with the external linear load (as supply torque meets demand thrust), and exceeding this 90-degree means that the linear load is too large or the rotating speed is too high, namely, the FTMC losing synchronization.

2.2. Theory and calculation

Based on the following assumptions: Firstly, disregarding the leaked axial flux in the air gap; secondly, neglecting the equivalent current volume of the magnet; and thirdly, overlooking the iron core reluctance. The instant thrust and torque of a single translator can be computed using the "swapped loading method" (Wang and Baker, 2018), the method is originally used in electric motor torque derivation by swapping functions of electric loading (magneto motive force per rotor perimeter in Ampere/meter) and magnetic loading (flux density in Tesla) which aims to simplify the difficulty of extracting air gap flux density profile from complex magnets array (Anglada and Sharkh, 2017). The calculation process for the FTMC is simplified as presented in

Eqs. (1)-(6) and elucidated in Figs. 6–8.

$$F = \int_0^{m_y} B_g \cdot I_{eq} \cdot l_f(y) dy \tag{1}$$

$$T = \int_0^{m_x} B_g \cdot I_{eq} \cdot r \cdot l_t(x) dx \tag{2}$$

$$B_g = B_0 / \left(1 + \frac{l_g \mu_r}{l_m} \right) \tag{3}$$

$$I_{eq} = (2 \cdot B_0 \cdot l_m) / (\mu_r \cdot \mu_0) \tag{4}$$

$$l_f(y) = \sum_{n=1,2 \dots 16} (I_n^+ - I_n^-) \tag{5}$$

$$l_t(x) = \sum_{n=1,2 \dots 16} (I_n^+ - I_n^-) \tag{6}$$

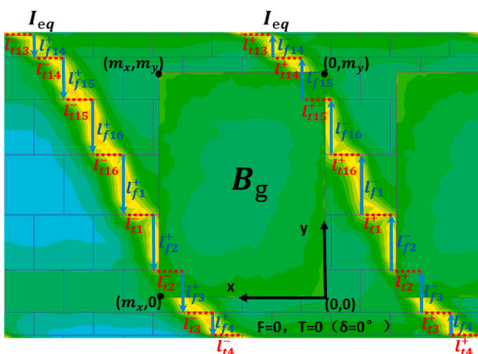


Fig. 6. Instant a: load angle $\delta = 0$ degrees, $F=0$; $T=0$.

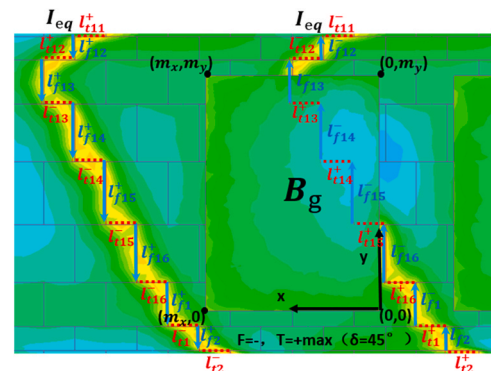


Fig. 7. Instant a: load angle $\delta = 45$ degrees, $F=-$; $T=+max$.

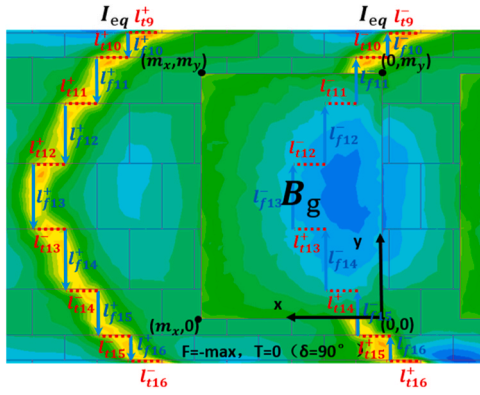


Fig. 8. Instant a: load angle $\delta = 90$ degrees, $F = -\max$ $T = 0$.

Where:

- F represents the thrust (N),
- T denotes the torque (Nm),
- B_g signifies the air gap flux density from the translator magnet (T),
- I_{eq} is the equivalent current of the rotor magnet (A),
- l_r and l_t denote the equivalent current conductor lengths of the rotor (m),
- r is the air gap radius (m),
- m_y and m_x represent the arc length and width of the translator magnet along the y and x axes (m),
- B_0 is the residual flux density of the magnet material (T),
- l_g is the equivalent air gap thickness (m),
- μ_r is the magnet relative permeability,
- l_m stands for the thickness of the translator and rotor magnet (m),
- and μ_0 is the per-unit permeability (H/m).

Fig. 6 illustrates the schematic diagram for the analysis of thrust and torque for translator 1 at instant a, with a load angle of 0 degrees. The positive (l_{r3}^+ , l_{r15}^+) and negative (l_{r15}^- , l_{r3}^-) equivalent current conductors of the rotor are symmetric and equal around the translator flux B_g region. Consequently, translator 1 experiences no thrust or torque.

In Fig. 7, the schematic diagram depicts the thrust and torque analysis for translator 1 at instant a, with a load angle of 45 degrees. The thrust component is determined by the projected length of the equivalent current conductors (l_{r13} , l_{r14} , l_{r15} , l_{r16}) in B_g region, while the torque component is determined by the projected length of the equivalent current conductors (l_{r13}^+ , l_{r14}^+ , l_{r15}^+) in B_g region. At this instant, the thrust component holds a negative value, and the torque component reaches a positive maximum value.

Fig. 8 showcases the schematic diagram for the analysis of thrust and torque for translator 1 at instant a, with a load angle of 90 degrees. The thrust equivalent current conductors include l_{r11} , l_{r12} , l_{r13} , l_{r14} , l_{r15} , and the torque equivalent current conductors are l_{r11}^- , l_{r12}^- , l_{r13}^+ , l_{r14}^+ . At this instant, the thrust component reaches a negative maximum value, and the torque components offset each other, resulting in a value of 0.

3. Results and discussion

3.1. Static performance

In Fig. 9, the 3D Finite Element Analysis (FEA) presents simulated thrust curves for nine characteristic instants ($\pm 25\%$, $\pm 50\%$, $\pm 75\%$, $\pm 100\%$, and 0 strokes) of translator 1. The y-axis represents translator thrust, and the x-axis indicates the rotor absolute angle. Detailed calculated data are listed in Table 1 for a comparison, demonstrating a well-matched validation of 96% overall accuracy. It's noteworthy from Table 1 that all data are centrosymmetrical to the central column (0% stroke, 180 degrees). By referencing Fig. 9 or Table 1, estimations of the

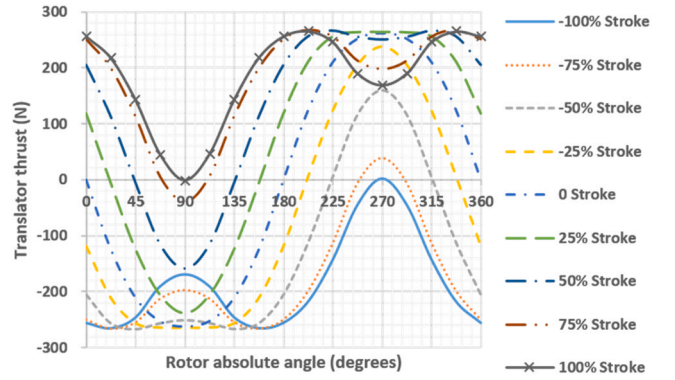


Fig. 9. Translator 1 thrust versus rotor absolute angle.

thrust curve for any translator at any instant with any load angle can be obtained (by determining the corresponding rotor absolute angle). Additionally, if the four translators operate symmetrically, their thrusts acting on the rotor cancel each other, resulting in a net thrust of 0. Fig. 10 displays FEA-simulated torque curves for the nine characteristic instants, with calculated results in Table 2. It's noteworthy from Table 2 that symmetrical stroke data are the same but with different phase shifts. The torque curve for any translator at any instant with any load angle can be derived from Fig. 10 or Table 2. However, the torque acting on the rotor is the negative sum of all four translators' torques.

Figs. 11–14 present key data of the FTMC. Fig. 11 illustrates thrust curves for all four translators at a load angle of 45 degrees. Fig. 12 depicts torque curves for all four translators and the combined rotor torque at a load angle of 45 degrees. Figs. 13–14 display thrust and torque curves for a load angle of 90 degrees. The y-axis represents thrust or torque, and the x-axis indicates the absolute rotor angle. The rotor torque is the sum of the four-translator torque, consistently maintained on the negative axis (Fig. 12), allowing the rotor to rotate in the same direction while translators reciprocate. Notably, the maximum load condition ($\delta = 90$ degrees, Fig. 13) does not significantly enhance driving thrust compared to the rated load condition ($\delta = 45$ degrees, Fig. 11), but it induces greater torque fluctuations (Fig. 14). The impact of the load angle on driving capacity follows a sinusoidal characteristic, similar to the MLS.

3.2. Dynamic performance and comparison

For both FTMC and MLS, while the rotor is driving the translator into a reciprocating motion, the acceleration and deceleration cost energy from the driver even in no-load condition, namely the translator loss. Assuming an ideal condition without frictional influence, the required driving thrust for the no-load condition is expressed in Eq. (7), where $F_{no-load}$ represents the required driving thrust (N), m is the translator mass (kg), l_s is the half stroke length (m), and f is the reciprocating frequency (Hz). The translator loss for a single motion cycle W_{loss} is calculated using Eq. (8), which implies that the area of the enclosed curve (driving thrust versus displacement) is the energy loss due to the acceleration and deceleration of the translator. Namely, the heavier the translator mass, the faster the frequency or the longer the stroke would lead to a higher energy loss.

$$F_{no-load} = m \cdot d^2 (l_s \cdot \sin(2\pi f t)) / dt^2. \quad (7)$$

$$W_{loss} = \oint_C F_{no-load} dl_s. \quad (8)$$

The driving transmission energy can be estimated by transforming the x-axis to the translator displacement in Fig. 11 and Fig. 13, creating enclosed thrust versus displacement curves as depicted in Fig. 15. A comparison of driving energy curves for different load angles with

Table 1
Data comparison of FEA and calculations for translator thrust.

Thrust N	-100 %		-75 %		-50 %		-25 %		0 %		25 %		50 %		75 %		100 %	
	FEA	Cal	FEA	Cal	FEA	Cal	FEA	Cal	FEA	Cal	FEA	Cal	FEA	Cal	FEA	Cal	FEA	Cal
0	-256	-250	-250	-255	-205	-200	-118	-93	0	0	118	93	205	200	250	255	256	250
22.5	-266	-265	-267	-265	-256	-250	-211	-199	-124	-101	-6	0	112	99	199	210	218	200
45	-246	-240	-255	-255	-266	-261	-256	-252	-210	-187	-124	-99	-6	0	113	99	143	130
67.5	-191	-185	-213	-220	-256	-252	-263	-265	-252	-245	-205	-189	-116	-98	6	0	45	45
90	-169	-169	-197	-210	-250	-241	-264	-265	-261	-265	-238	-230	-159	-165	-39	-40	-1	0
112.5	-191	-185	-213	-220	-255	-252	-263	-265	-252	-245	-205	-189	-116	-98	6	0	45	45
135	-246	-240	-255	-255	-266	-261	-255	-252	-210	-187	-124	-99	-5	0	113	99	143	130
157.5	-265	-265	-266	-265	-256	-250	-211	-199	-124	-101	-6	0	113	99	199	210	218	200
180	-256	-250	-250	-255	-205	-200	-118	-93	0	0	119	93	205	200	251	255	256	250
202.5	-218	-200	-199	-210	-112	-99	6	0	125	101	211	199	256	250	267	265	266	265
225	-143	-130	-113	-99	5	0	124	99	210	187	256	252	266	261	255	255	246	240
247.5	-45	-45	-6	0	116	98	205	189	252	245	263	265	255	252	212	220	190	185
270	2	0	39	40	160	165	238	230	262	265	264	265	250	241	197	210	169	169
292.5	-45	-45	-6	0	116	98	205	189	252	245	263	265	255	252	212	220	190	185
315	-143	-130	-113	-99	5	0	124	99	210	187	256	252	266	261	255	255	246	240
337.5	-218	-200	-199	-210	-112	-99	6	0	124	101	211	199	256	250	266	265	265	265
360	-256	-250	-250	-255	-205	-200	-118	-93	0	0	118	93	205	200	250	255	256	250

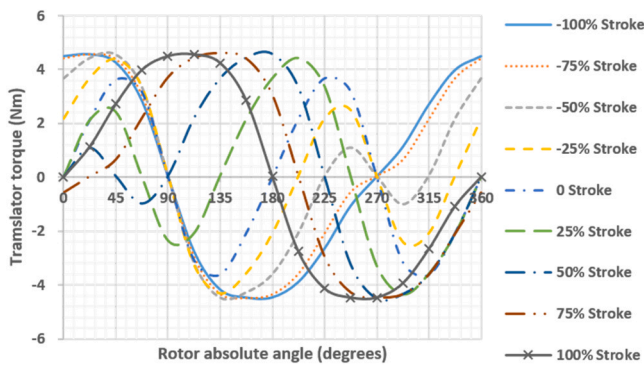


Fig. 10. Translator 1 torque versus rotor absolute angle.

energy loss curves for different frequencies reveals that a single FTMC translator can ideally achieve a maximum 30 Hz no-load reciprocating motion with a 45-degree load angle and 36.5 Hz reciprocating motion with a 90-degree load angle.

Similar to the FTMC translator, the MLS rotor loss for a single motion cycle W_{rloss} is estimated through Eqs. (9)–(11). Where, $T_{no-load}$ represents the required driving torque (Nm), J is the rotor inertia (kg·m²), l_r is the quarter angular length (1.57 rad), f is the reciprocated rotating

frequency (Hz), m is the rotor mass (kg), and r is the rotor radius (m).

$$T_{no-load} = J \cdot d^2(l_r \cdot \sin(2\pi ft)) / dt^2. \tag{9}$$

$$J = m \cdot r^2 / 2. \tag{10}$$

$$W_{rloss} = \oint_C T_{no-load} dl_r. \tag{11}$$

Fig. 16 illustrates that to achieve the same frequency as the FTMC, a same-sized MLS rotor needs to overcome a significant rotor loss as the frequency increases. It's crucial to note that rotor loss is exclusive to the MLS, limiting the maximum working speed even with a larger static thrust. Although the FTMC rotor also has rotor loss due to the torque ripple, the quantity is not comparable to the MLS. As shown in Fig. 17 is an energy loss comparison between MLS and FTMC at 30 Hz for a single motion cycle, where the x-axis represents the angular position and the y-axis represents the torque, the dashed line covered shadow area represents the energy that will transmit to the translator and the solid line covered shadow area represents the required energy loss that supports the acceleration and deceleration of the rotor. It can be seen that the unidirectional rotary motion of the FTMC has a considerable advantage on transmission efficiency (much less rotor loss) compared to the bidirectional rotary motion of the MLS in high-speed motion. What is more, since the FTMC rotor only has one directional torque and maintains unidirectional rotary motion (near constant speed), its dashed line

Table 2
Data comparison of FEA and calculations for translator torque.

Torque Nm	-100 %		-75 %		-50 %		-25 %		0 %		25 %		50 %		75 %		100 %	
	FEA	Cal	FEA	Cal	FEA	Cal	FEA	Cal	FEA	Cal	FEA	Cal	FEA	Cal	FEA	Cal	FEA	Cal
0	4.5	4.3	4.4	4.5	3.7	3.5	2.2	1.9	0.0	0.0	0.0	0.0	0.0	0.0	-0.6	-0.3	0.0	0.0
22.5	4.6	4.5	4.6	4.8	4.4	4.5	3.7	3.5	2.1	2.6	2.1	1.9	1.1	1.0	0.0	0.0	1.1	0.9
45	4.3	4.1	4.4	4.5	4.6	4.7	4.4	4.1	3.6	3.7	2.4	2.6	0.1	0.0	0.7	0.9	2.7	2.5
67.5	2.8	2.5	3.1	2.9	3.4	2.9	3.4	3.0	3.2	2.6	0.0	0.0	-1.0	-1.0	2.2	2.2	4.0	3.7
90	0.0	0.0	0.1	0.0	0.0	0.0	0.1	0.0	0.0	0.0	-2.3	-1.9	0.1	0.0	3.7	3.5	4.5	4.3
112.5	-2.7	-2.5	-2.9	-2.9	-3.2	-2.9	-3.3	-3.5	-3.1	-2.6	-2.1	-1.9	2.2	1.9	4.4	4.5	4.6	4.5
135	-4.2	-4.0	-4.3	-4.5	-4.5	-4.7	-4.3	-4.0	-3.6	-3.7	0.1	0.0	3.7	3.5	4.6	4.8	4.2	4.1
157.5	-4.5	-4.4	-4.5	-4.7	-4.3	-4.5	-3.6	-3.5	-2.1	-2.6	2.2	1.9	4.5	4.5	4.4	4.5	2.9	2.5
180	-4.5	-4.3	-4.3	-4.5	-3.6	-3.3	-2.1	-1.9	0.0	0.0	3.7	3.5	4.6	4.7	3.1	2.9	0.0	0.0
202.5	-3.9	-3.5	-3.6	-3.2	-2.1	-1.9	0.1	0.0	2.2	2.6	4.4	4.1	3.3	2.9	0.0	0.0	-2.8	-2.5
225	-2.6	-2.5	-2.1	-1.9	0.0	0.0	2.2	1.9	3.7	3.7	3.4	3.0	0.1	0.0	-2.9	-2.9	-4.1	-4.0
247.5	-1.1	-0.9	-0.5	-0.3	1.1	1.0	2.5	2.6	3.2	2.6	0.1	0.0	-3.2	-2.9	-4.3	-4.5	-4.5	-4.4
270	0.0	0.0	0.1	0.0	0.0	0.0	0.1	0.0	0.0	0.0	-3.3	-3.5	-4.5	-4.7	-4.5	-4.7	-4.5	-4.3
292.5	1.1	0.9	0.7	0.9	-1.0	-1.0	-2.4	-1.9	-3.1	-2.6	-4.3	-4.0	-4.3	-4.5	-4.3	-4.5	-3.9	-3.5
315	2.7	2.5	2.2	2.2	0.1	0.0	-2.1	-1.9	-3.6	-3.7	-3.6	-3.5	-3.6	-3.3	-3.6	-3.2	-2.7	-2.5
337.5	4.0	3.7	3.7	3.5	2.2	1.9	0.1	0.0	-2.1	-2.6	-2.1	-1.9	-2.1	-1.9	-2.1	-1.9	-1.1	-0.9
360	4.5	4.3	4.4	4.5	3.7	4.0	2.2	1.9	0.0	0.0	0.0	0.0	0.0	0.0	-0.6	-0.3	0.0	0.0

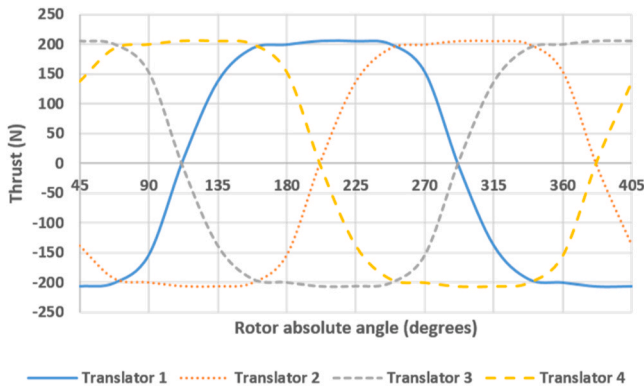


Fig. 11. Thrust versus rotor absolute angle ($\delta=45$).

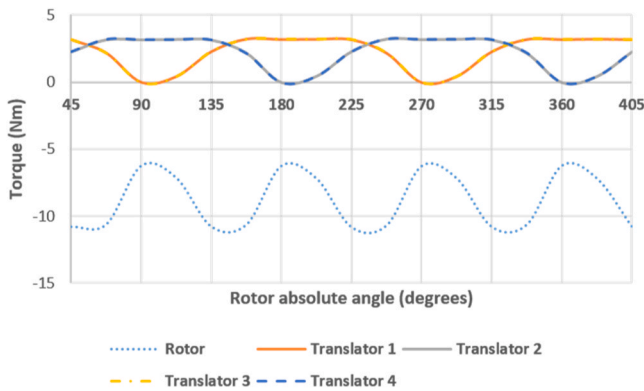


Fig. 12. Torque versus rotor absolute angle ($\delta=45$).

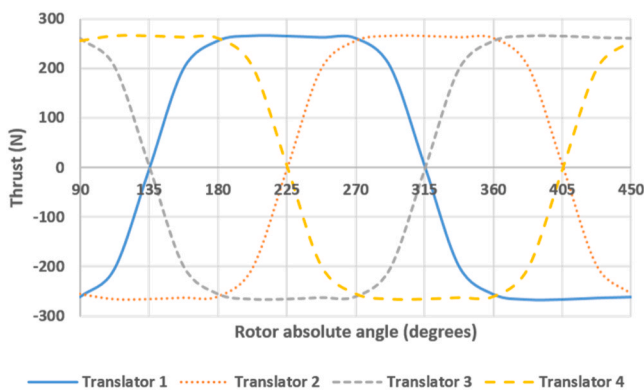


Fig. 13. Thrust versus rotor absolute angle ($\delta=90$).

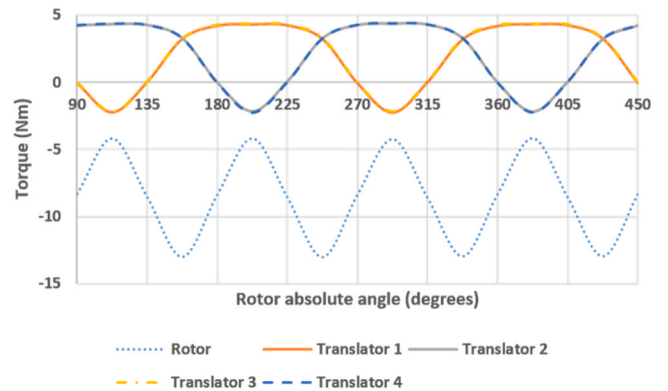


Fig. 14. Torque versus rotor absolute angle ($\delta=90$).

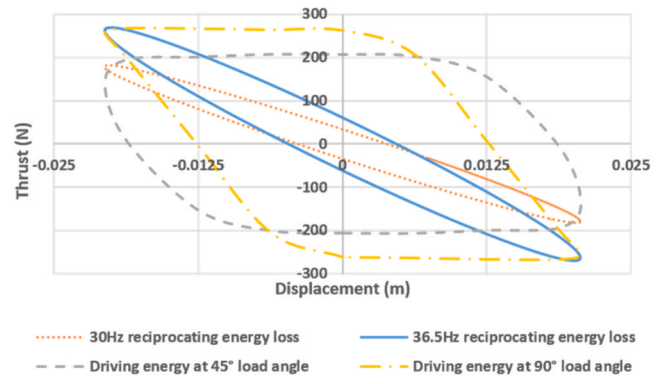


Fig. 15. FTMC single translator no-load dynamic limitations.

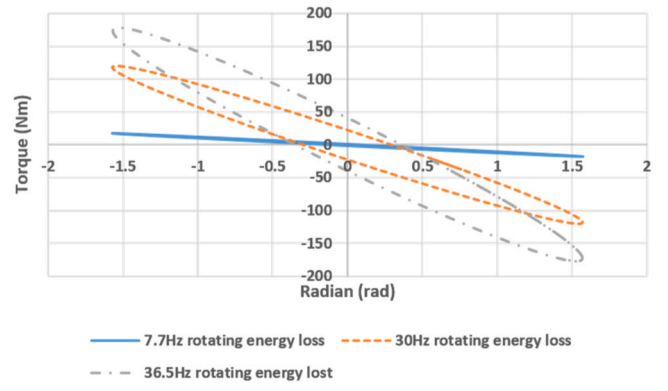


Fig. 16. MLC counterpart extra rotor loss.

covered shadow area also implies the stored energy on the FTMC rotor is always constant for the whole single motion cycle.

Table 3 below provides a clearer data comparison. For the same-sized FTMC and MLS based on their maximum static torque, the FTMC (4.6 m/s) can achieve 4.6 times the maximum reciprocating speed of the MLS (1.0 m/s). Alternatively, the FTMC (13.0 Nm) only requires 6.7 % of the peak driving torque of the MLS (194.9 Nm) when forcing the translator to the same 36.5 Hz.

3.3. Assembly performance prediction

The design of the FTMC, featuring four translators, draws inspiration from the working principle of a four-cylinder engine (Bush et al., 2000; Mishra, 2013), the aiming to enhance the reciprocating speed compared

to conventional MLS systems. In contrast to the MLS, the FTMC boasts advantages such as high efficiency, high frequency, high power, and ideally no rotor backlash. However, a foreseeable drawback is the radial attraction of the translator induced by the rotor magnet, potentially increasing friction with bearings. As depicted in Fig. 18, the original topology comprises a single air gap. The 2-air gap topology is developed by separating the core backs of the four translators from the magnets and reuniting them as a single stator. In comparison to the 1-air gap topology, the 2-air gap topology offers two main advantages:

- 1) It not only offsets core attraction but also minimizes attraction between magnets. As illustrated in Fig. 19, the 1-air gap topology (6 mm air gap) exhibits a peak radial attraction of 646 N on each translator, while the 2-air gap topology (3 mm inside and 3 mm outside) reduces the peak attraction to 277 N. Further optimization,

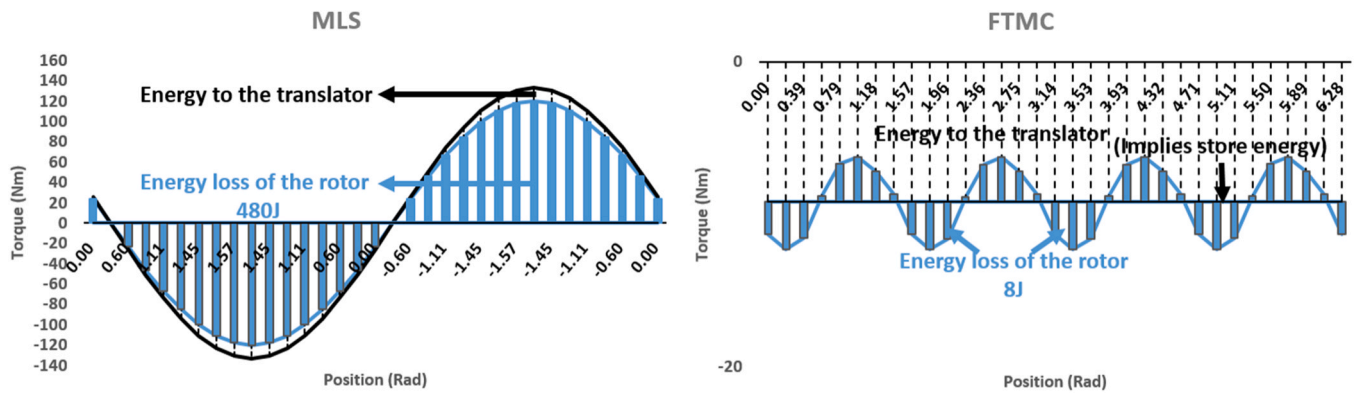


Fig. 17. Rotor's energy loss comparison between MLS and FTMC at 30 Hz (single motion cycle).

Table 3 Same-sized FTMC & MLC key data comparison.

Parameters	FTMC	MLS
Translator mass	0.25Kg (Single translator)	1Kg
Rotor mass	4.22Kg (inertia 0.022 kg·m ²)	
Rated peak thrust	206 N (Single translator)	824 N
Maximum peak thrust	267 N (Single translator)	1068 N
Rated peak torque	10.9Nm	12.8Nm
Maximum peak torque	13.0Nm	17.3Nm
Maximum reciprocating speed	4.6 m/s (36.5 Hz)	1.0 m/s (7.7 Hz)
Minimum driving torque for 36.5 Hz	13.0Nm	194.9Nm

2) The translator's mass is significantly reduced (0.25 kg as listed in Table 3), enhancing reciprocating frequency and driving efficiency.

A preliminary assembly strategy is presented in Fig. 20, where four translators are positioned on four shafts, four shafts are positioned on two shaft holders on each side, and then these are regarded as a single unit to install within the tubular stator core, the stator core is positioned between two stator end cups with mounting studs and nuts to fix the radial position. What is more, the rotor is located between the two stator end cups with ball bearings to support its rotary motion, some magnets related axial dimensions are also presented in Fig. 20. A more detailed translator rail design with radial dimensions marked is shown in Fig. 21, where translator magnets are installed on the translator base, the translator base is installed on two symmetric sides of the shafts with balls attached between them, and the ball container contains balls. Excluding friction and assembly deviations, Table 4 below presents the anticipated performance of the FTMC under ideal working conditions, where the translator load consistently aligns with the rotor input to maintain a constant load angle δ . All data are inferred from highly precise and calculation-validated static 3D FEA results. The FTMC demonstrates the ability to achieve approximately 1.4 kW power transmission to the load with a 77 % efficiency at 30 Hz (rated load $\delta=45$ degrees) and 1.2 kW power with 63 % efficiency at 36.5 Hz (maximum load $\delta=90$ degrees).

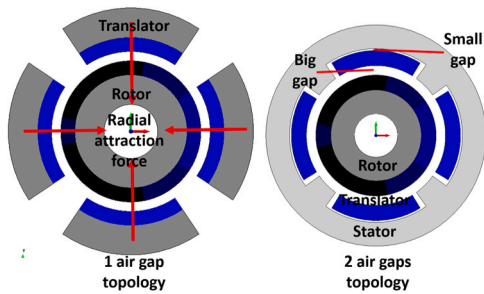


Fig. 18. 1 air gap and 2 air gaps topologies.

4. Conclusions

In conclusion, this study introduces a ground breaking mechanism known as the Four-Translator Magnetic Crankshaft (FTMC), which amalgamates features from the Magnetic Lead Screw (MLS) and the traditional cross crankshaft. The FTMC allows for seamless conversion between continuous rotational motion and reciprocating motion, boasting a pivotal technological advancement with its rotor's energy storage capabilities. The paper systematically covers the mechanism's introduction, working principle, calculation methodology, 3D finite element analysis (FEA) validation, dynamic comparison, and assembly design.

Notable findings include the FTMC's ability to achieve over 4.6 times the maximum reciprocating speed of an MLS with the same driving force, or require only 6.7 % of the driving torque needed by an MLS at the same reciprocating speed. The study provides comprehensive static and dynamic performance analyses, revealing the FTMC's efficiency, frequency, and power advantages over conventional MLS systems.

Additionally, the study proposes a novel assembly design, addressing potential defects such as radial attraction of the translator and providing solutions through a 2-air gap topology. The anticipated performance of the FTMC under ideal working conditions, derived from precise static 3D FEA results, predicts its ability to achieve approximately 1.4 kW power transmission with a 77 % efficiency at 30 Hz (rated load $\delta=45$ degrees)

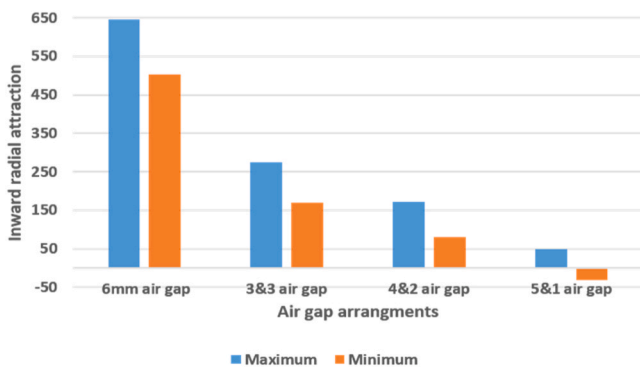


Fig. 19. Air gap rearrangement influence on radial attractions.

with a 2-air gap topology of 4 mm inside and 2 mm outside, lowers the attraction to 159 N. The final optimized topology (5 mm inside and 1 mm outside) achieves a minimal 50 N attraction.

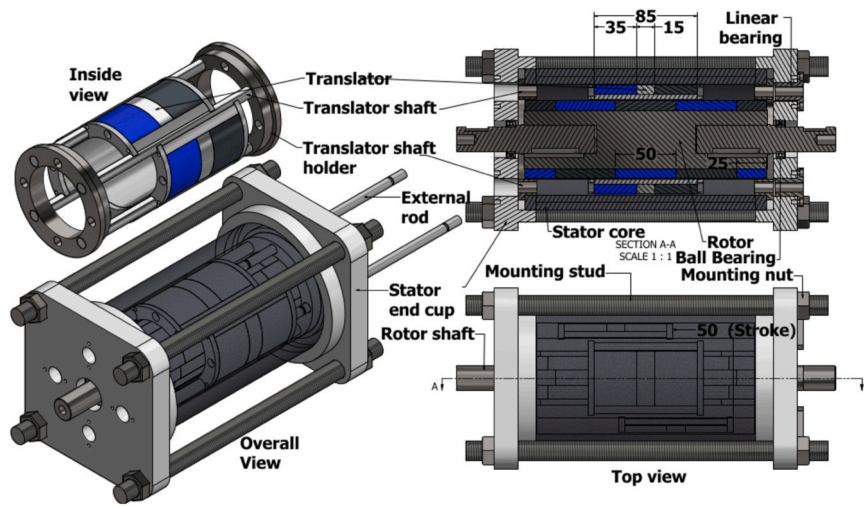


Fig. 20. General assembly strategy.

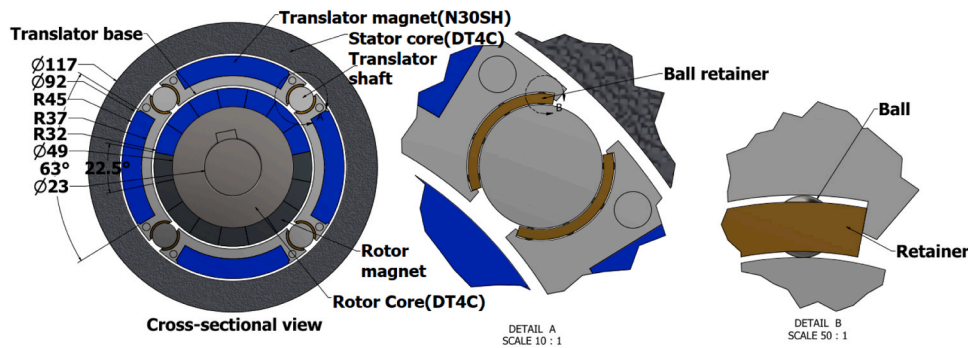


Fig. 21. Key feature of the assembly strategy.

Table 4
Predicted FTMC performance summary.

Conditions	Parameters	Values
Rated load ($\delta=45$)	Maximum peak thrust	206 N
	Energy input for 1 cycle	60.7 J
	Energy loss on translator for 1 cycle	14.1 J
	Maximum frequency	30 Hz
	Input mean power	1820.4 W
	Load mean power	1398.3 W
	Efficiency	76.8 %
Maximum load ($\delta=90$)	Maximum peak thrust	267 N
	Energy input for 1 cycle	53.0 J
	Energy loss on translator for 1 cycle	19.8 J
	Maximum frequency	36.5 Hz
	Input mean power	1934.5 W
	Load mean power	1210.9 W
	Efficiency	62.6 %

and 1.2 kW power with 63 % efficiency at 36.5 Hz (maximum load $\delta=90$ degrees).

This theoretical exploration of the Magnetic Crankshaft (MC) presents a promising avenue for future research and prototyping efforts. The FTMC mechanism, if validated through experiments, is poised to play a significant role in advancing Magnetic Lead Screw (MLS) and high-speed magnetic drive systems. Future studies are recommended to focus on prototype manufacturing and controllable load test bench design to validate the maximum driving ability of the FTMC mechanism listed in the presented analysis.

CRediT authorship contribution statement

Junnan Wang: Writing – review & editing, Writing – original draft, Visualization, Validation, Supervision, Software, Resources, Project administration, Methodology, Investigation, Funding acquisition, Formal analysis, Data curation, Conceptualization. **Yaodong Wang:** Writing – review & editing, Writing – original draft, Visualization, Validation, Supervision.

Declaration of Competing Interest

The authors declare the following financial interests/personal relationships which may be considered as potential competing interests: Junnan Wang reports financial support was provided by Jiangsu Province Natural Science Foundation. If there are other authors, they declare that they have no known competing financial interests or personal relationships that could have appeared to influence the work reported in this paper.

Data Availability

Data will be made available on request.

Acknowledgment

This study was supported in part by the Jiangsu Natural Science Foundation under grant No.BK20200141.

References

- Anglada, J.R., Sharkh, S.M., 2017. An insight into torque production and power factor in transverse-flux machines (May-June). *IEEE Trans. Ind. Appl.* vol. 53 (3), 1971–1977. <https://doi.org/10.1109/TIA.2017.2665344>.
- Bo, W., Qiang, Z., Ting, L., Yizhuo, J., 2022. Modal analysis of a V-type engine crankshaft based on workbench. 2022 IEEE International Conference on Electrical Engineering, Big Data and Algorithms (EEBDA). Changchun, China, pp. 1154–1156. <https://doi.org/10.1109/EEBDA53927.2022.9744758>.
- Bush, Phillip, et al., 2000. A design strategy for four cylinder SI automotive engine exhaust systems (Jan.). SAE Trans. 659–671 (Jan.).
- Csere, 2023. Csaba. Different Stroke: Could the light and compact e-REX from the Spanish company INNengine be the EV range extender of the future? *Car Driv.* 69 (5), 16–17.
- Guo, H., Li, Y., Zhang, X., 2018. Development of a performance test platform of direct-drive servo valve linear force motor. *2018 15th International Conference on Ubiquitous Robots (UR)*. Honolulu, HI, USA, pp. 781–785. <https://doi.org/10.1109/URAI.2018.8441779>.
- Holm, R.K., Berg, N.I., Walkusch, M., Rasmussen, P.O., Hansen, R.H., 2013. Design of a magnetic lead screw for wave energy conversion (Nov.-Dec.). *IEEE Trans. Ind. Appl.* vol. 49 (6), 2699–2708. <https://doi.org/10.1109/TIA.2013.2264272>.
- Jenney, K., Pakdelian, S., 2020. Magnetic design aspects of the trans-rotary magnetic gear using quasi-halbach arrays (Nov.). *IEEE Trans. Ind. Electron.* vol. 67 (11), 9582–9592. <https://doi.org/10.1109/TIE.2019.2955424>.
- Lorimer, W., Hartman, A., 1997. Magnetization pattern for increased coupling in magnetic clutches (Sept.). *IEEE Trans. Magn.*, vol. 33 (5), 4239–4241. <https://doi.org/10.1109/20.619722>.
- Maia, Fabricius Viana, Gabriel Macedo, and Fábio Sirbone. Finite Element Analysis for Estimation of Internal Loads in a Shift Drum System No. 2014-36-0242. SAE Technical Paper, 2014.
- Mishra, P.C., 2013. Modeling for friction of four stroke four cylinder in-line petrol engine. *Tribology Ind.* 35 (3), 237.
- Mustafa, D., Hussain, H.A., 2023. A review and comparative study on the design and analysis of magnetic lead screws (July-Aug). *IEEE Trans. Ind. Appl.* vol. 59 (4), 4108–4119. <https://doi.org/10.1109/TIA.2023.3270270>.
- R. Safarpour and S. Pakdelian, Topology Optimization of the Reluctance Trans-Rotary Magnetic Gear, in *IEEE Transactions on Magnetics*, vol. 58, no. 2, pp. 1-5, Feb. 2022, Art no. 8102805, doi: [10.1109/TMAG.2021.3085509](https://doi.org/10.1109/TMAG.2021.3085509).
- Thi, N.H., Trang, N.V., Cong, H.T., Loc, H.V., Huy, D.H., Huy, N.D., 2020. A preliminary study of a two stroke free-piston engine for electricity generation. *2020 5th International Conference on Green Technology and Sustainable Development (GTSD)*. Ho Chi Minh City, Vietnam, pp. 669–672. <https://doi.org/10.1109/GTSD50082.2020.9303112>.
- Wang, J., Atallah, K., Wang, W., 2011. Analysis of a magnetic screw for high force density linear electromagnetic actuators (Oct.). *IEEE Trans. Magn.*, vol. 47 (10), 4477–4480. <https://doi.org/10.1109/TMAG.2011.2157464>.
- Wang, J., Baker, N.J., 2018. A linear laminated cylindrical transverse flux machine for use with a free piston engine (Dec.). *IEEE Trans. Energy Convers.* vol. 33 (4), 1988–1997. <https://doi.org/10.1109/TEC.2018.2877502>.